Developmental origin and maintenance of distinct testicular macrophage populations

Noushin Mossadegh-Keller,[1] Rebecca Gentek,[1] Gregory Gimenez,[1,2] Sylvain Bigot,[1] Sebastien Mailfert,[1] and Michael H. Sieweke[1,2]

[1]Centre d'Immunologie de Marseille-Luminy, Aix Marseille University, Centre National de la Recherche Scientifique, Institut National de la Santé et de la Recherche Médicale, Marseille, France
[2]Max-Delbrück-Centrum für Molekulare Medizin in der Helmholtzgemeinschaft, Berlin, Germany

Testicular macrophages (tMφ) are the principal immune cells of the mammalian testis. Beyond classical immune functions, they have been shown to be important for organogenesis, spermatogenesis, and male hormone production. In the adult testis, two different macrophage populations have been identified based on their distinct tissue localization and morphology, but their developmental origin and mode of homeostatic maintenance are unknown. In this study, we use genetic lineage–tracing models and adoptive transfer protocols to address this question. We show that embryonic progenitors give rise to the interstitial macrophage population, whereas peritubular macrophages are exclusively seeded postnatally in the prepuberty period from bone marrow (BM)–derived progenitors. As the proliferative capacity of interstitial macrophages declines, BM progenitors also contribute to this population. Once established, both the peritubular and interstitial macrophage populations exhibit a long life span and a low turnover in the steady state. Our observations identify distinct developmental pathways for two different tMφ populations that have important implications for the further dissection of their distinct roles in organ homeostasis and testicular function.

INTRODUCTION

Macrophages are innate immune cells that are present in essentially all organs of the body. Besides their diverse role in shaping the immune response, they have trophic functions in tissue homeostasis and regeneration and contribute to many organ-specific functions (Wynn et al., 2013), including in the gonads (Shechter et al., 2013; Smith et al., 2015).

In males, the testis are the site of spermatogenesis and male hormone production and can maintain fertility and virility over an extended reproductive period. Testicular macrophages (tMφ) represent the most abundant immune cells in the organ (Winnall and Hedger, 2013) and contribute to organ function in several ways. As spermatogenesis is only initiated at puberty and sperm-specific neoantigens become expressed after the education of the immune system, the testis requires a mechanism of self-tolerance to these antigens. TMφ contribute to maintaining an immunoprivileged environment in the organ by the production of immunosuppressive cytokines, such as IL-10 and TGF-β, and by low expression of proinflammatory cytokines (Fijak and Meinhardt, 2006; Shechter et al., 2013). TMφ are also intimately associated with Leydig cells and play an important role in their development, regeneration, and testosterone production (Hutson, 1998; Smith et al., 2015). Whereas this macrophage population resides in the interstitial space between seminiferous tubes, a peritubular population has recently been identified that is associated directly with spermatogonial tubes in proximity to spermatogonial stem cells (SSCs). This has been suggested to have an effect on the SSC niche and a potential functional role in SSC differentiation (DeFalco et al., 2015).

Despite these proposed important functional roles, relatively little is known about the development and maintenance of tMφ. It was originally thought that tissue macrophages were principally derived from blood monocytes developing from hematopoietic stem cells in the BM (van Furth and Cohn, 1968), but this view has changed when different genetic-, genomic-, and fate-mapping studies showed that macrophages of different organs can also be derived from embryonic progenitors (Ginhoux et al., 2010; Hoeffel et al., 2012; Schulz et al., 2012; Hashimoto et al., 2013; Yona et al., 2013; Gomez Perdiguero et al., 2015; Hagemeyer et al., 2016; Mass et al., 2016), which seed the organs at different stages of development and self-maintain independently of BM contribution into adulthood (Ajami et al., 2007; Hashimoto et al., 2013; Sieweke and Allen, 2013; Gomez Perdiguero et al., 2015). Autonomous macrophage self-renewal capacity depends on a network of specific self-renewal genes shared with stem cells (Aziz et al., 2009; Soucie et al., 2016). Depending on the organ, embryonic-derived macrophages can get par-

Correspondence to Michael H. Sieweke: sieweke@ciml.univ-mrs.fr

Abbreviations used: HS/PC, hematopoietic stem and progenitor cell; IF, immunofluorescence; SSC, spermatogonial stem cell; TAM, tamoxifen; tMϕ, testicular macrophages.

The Rockefeller University Press
J. Exp. Med. 2017 Vol. 214 No. 10 2829–2841
https://doi.org/10.1084/jem.20170829

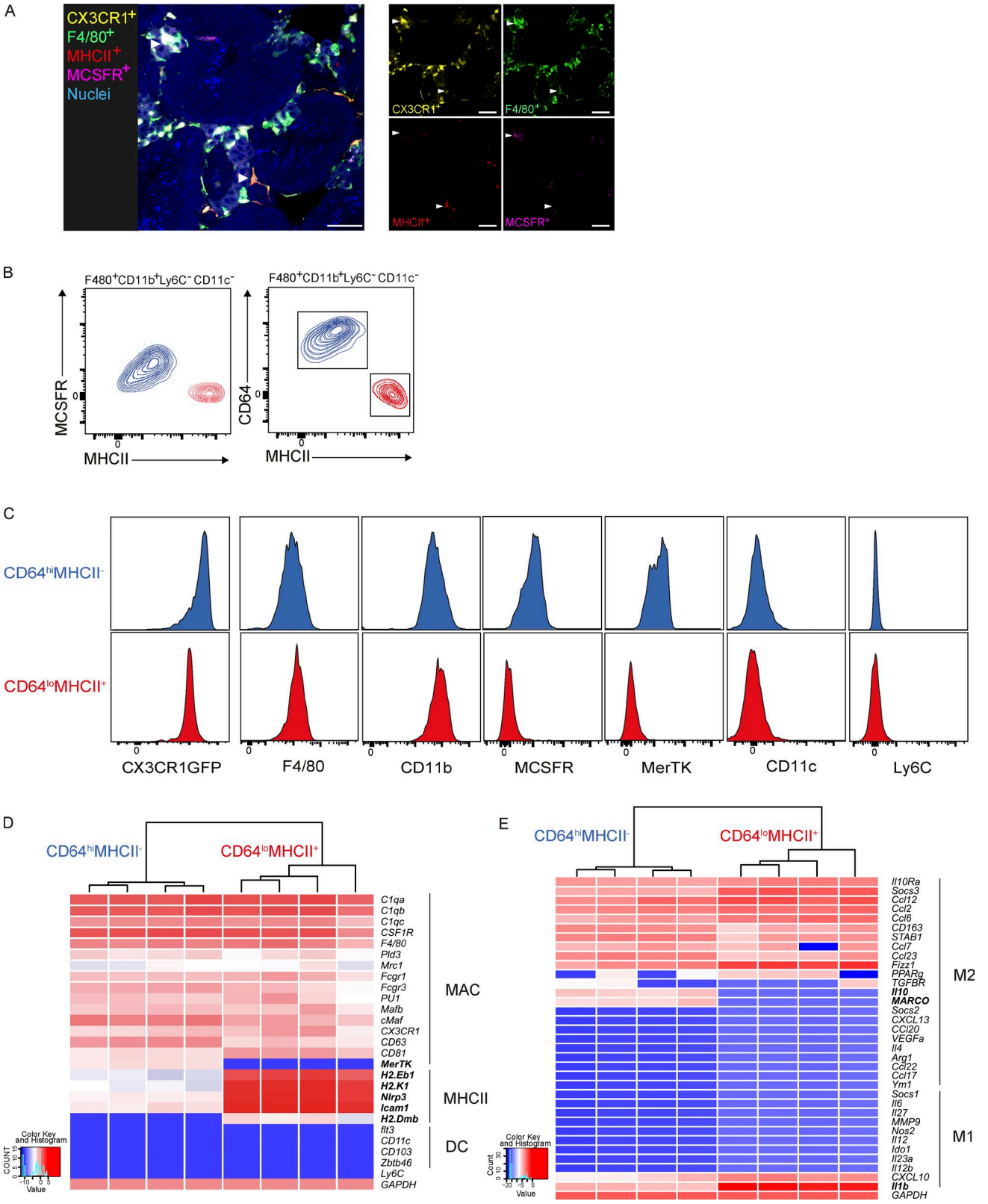

Figure 1. **Phenotypic characterization of two tMφ populations by cell-surface marker and gene expression profiling.** (A) IF imaging of 16-wk-old CX3CR1-GFP mouse testis showing morphology, localization, M-CSFR, and MHCII staining of interstitial tMφ and peritubular tMφ, indicated with arrowheads. Bars, 40 µm. (B) Representative FACS profiles of adult mouse F4/80^{+}CD11b^{+}Ly6C^{-}CD11c^{-} tMφ populations showing that both CD64 and M-CSFR

tially or fully replaced by BM-derived macrophages in the adult tissues (Tamoutounour et al., 2012; Bain et al., 2014; Epelman et al., 2014; Molawi et al., 2014). For example, we have shown previously that embryo-derived cardiac macrophages loose self-renewal capacity with age and are successively replaced by BM-derived macrophages in adulthood (Molawi et al., 2014). Here, we have now characterized postnatal development and the origin of tMφ.

During the initial phases of testis morphogenesis in early embryonic development from E10.5 to E14.5, yolk sac–derived macrophages are associated with nascent gonadal and mesonephric vasculature and are required for vascular remodeling (DeFalco et al., 2014). In the adult testis, two different macrophage populations have been distinguished by their morphology, their M-CSFR and MHCII expression profiles, and their localization in the interstitium or the surface of seminiferous tubules (DeFalco et al., 2015). However, it is not known whether these two macrophage populations are derived from early embryonic tMφ or whether they have distinct origins and arise independently. Here, we examined the postnatal development dynamics, the turnover, and the specific origin of these two tMφ populations. Combining genetic lineage tracing and a neonatal adoptive transfer model, we demonstrate that embryo-derived macrophages persist into the postnatal testis, where they selectively contribute only to the interstitial population but are partially replenished from BM-derived progenitors at later stages, when local expansion has declined. Peritubular tMφ, however, only emerge postnatally from BM-derived progenitors in the prepuberty period. Once established, the two populations exhibit long life span and low turnover in the adult testis at steady state.

RESULTS AND DISCUSSION

We initially characterized the macrophage populations present in testis by immunofluorescence (IF). Consistent with previous observations (DeFalco et al., 2015), we observed that tMφ were positive for CX3CR1 and F4/80 but that two populations could be distinguished based on their peritubular and interstitial locations, which were M-CSFR positive and MHCII negative or M-CSFR negative and MHC II positive, respectively (Fig. 1 A). We further characterized these two interstitial (M-CSFR$^+$MHCII$^-$) and peritubular (M-CSFR^{lo}MHCII$^+$) tMφ populations by flow cytometry (FACS), using an extended antibody panel that excluded infiltrating leukocytes (Fig. S1). Within the testicular leukocytes fraction (CD45$^+$), resident macrophages were defined as Ly6C$^-$ CD11c$^-$ F4/80$^+$ CD11b$^+$ cells (Fig. S1). We also analyzed the expression of additional tissue-resident macrophage markers CX3CR1, CD64, and MerTK (Gautier et al., 2012). We found that interstitial (MCSFR$^+$MHCII$^-$) and peritubular (M-CSFR^{lo}MHCII$^+$) tMφ could be interchangeably and clearly distinguished by differential expression of CD64 and MHCII (Fig. 1, B and C). The two populations also expressed differential levels of MerTK but were both positive for CX3CR1. Although both populations were negative for CD11c (Fig. 1 B), the absence of the core macrophage markers CD64 and MerTK in peritubular CD64^{lo}MHC II$^+$ macrophages prompted us to analyze macrophage- and DC-specific gene expression in the two populations in more depth. We investigated the expression of several core macrophage-associated factors (*C1qa*, *C1qb*, *C1qc*, *CSF1R*, *F4/80*, *Pld3*, *Mrc1*, *Fcgr1*, *Fcgr3*, *Pu1*, *Mafb*, *cMaf*, *CXC3CR1*, *CD81*, *CD63*, and *MerTK*), factors regulating antigen processing and presentation (*H2.Dmb*, *H2.Eb1*, *Nlrp3*, *H2.K1*, and *Icam1*; Epelman et al., 2014), and DC markers (*CD103*, *Zbtb46*, *Flt3*, and *CD11c*), using nanofluidic Fluidigm array real-time PCR (Fig. 1 D). Both M-CSFR$^+$CD64^{hi}MHCII$^-$ interstitial and M-CSFR^{lo}CD64^{lo}MHCII$^+$ peritubular macrophages expressed all analyzed macrophage markers, except *MerTK*, which was absent in CD64^{lo}MHCII$^+$ macrophages. In contrast, the expression of genes regulating antigen processing and presentation was up-regulated in this population. The DC markers tested were not expressed by either population, clearly identifying both of them as macrophages. As spermatogenesis occurs after the maturation of the immune system and the establishment of systemic tolerance, the developing gametes in the testis need to be protected from autoimmune attack. Establishment and maintenance of immune tolerance in the testis has, at least in part, been attributed to an antiinflammatory phenotype of tMφ (Fijak and Meinhardt, 2006; Shechter et al., 2013), but it has not been established whether both tMφ populations have an immunosuppressive phenotype and which pathways might be differentially engaged. Therefore, we analyzed CD64^{hi}MHCII$^-$ interstitial and CD64^{lo}MHCII$^+$ peritubular tMφ populations for the expression of proinflammatory genes characteristic of a classical M1-type activation or several immunosuppressive *IL-10*–, *TGF-β*–, and *IL-4*–dependent alternative M2-type activation pathways (Murray et al., 2014). The two populations showed highly similar gene expression profiles with the absence of proinflammatory gene expression but the expression of a large number of immunosuppressive and alternative M2-type acti-

staining distinguishes CD64^{hi} or M-CSFR$^+$MHCII$^-$ (interstitial; blue) and CD64^{lo} or M-CSFR$^-$MHCII$^+$ (peritubular; red) populations in adult testes. (C) Analysis of expression levels of core macrophage cell-surface markers in CD45$^+$F4/80$^+$CD11b$^+$ tMφ for CX3CR1-GFP levels and in CD45$^+$CX3CR1GFP$^+$ for F4/80, CD11b, MCSFR, and MerTK in interstitial CD64^{hi}MHCII$^-$ and peritubular CD64^{lo}MHCII$^+$ tMφ. (A–C) Data are representative of two independent experiments. (D) Gene expression analysis of interstitial (CD64^{hi}MHCII$^-$) and peritubular (CD64^{lo}MHCII$^+$) tMφ isolated from four individual wild-type mice. Expression levels of macrophage-related genes, genes regulating antigen processing and presentation, and DC-related genes were determined using nanofluidic Fluidigm array real-time PCR. MAC, macrophage. (E) Gene expression analysis on the same populations as in D for M2 and M1 macrophage activation-related genes by nanofluidic Fluidigm array real-time PCR. Genes in bold show the difference between the two testicular populations.

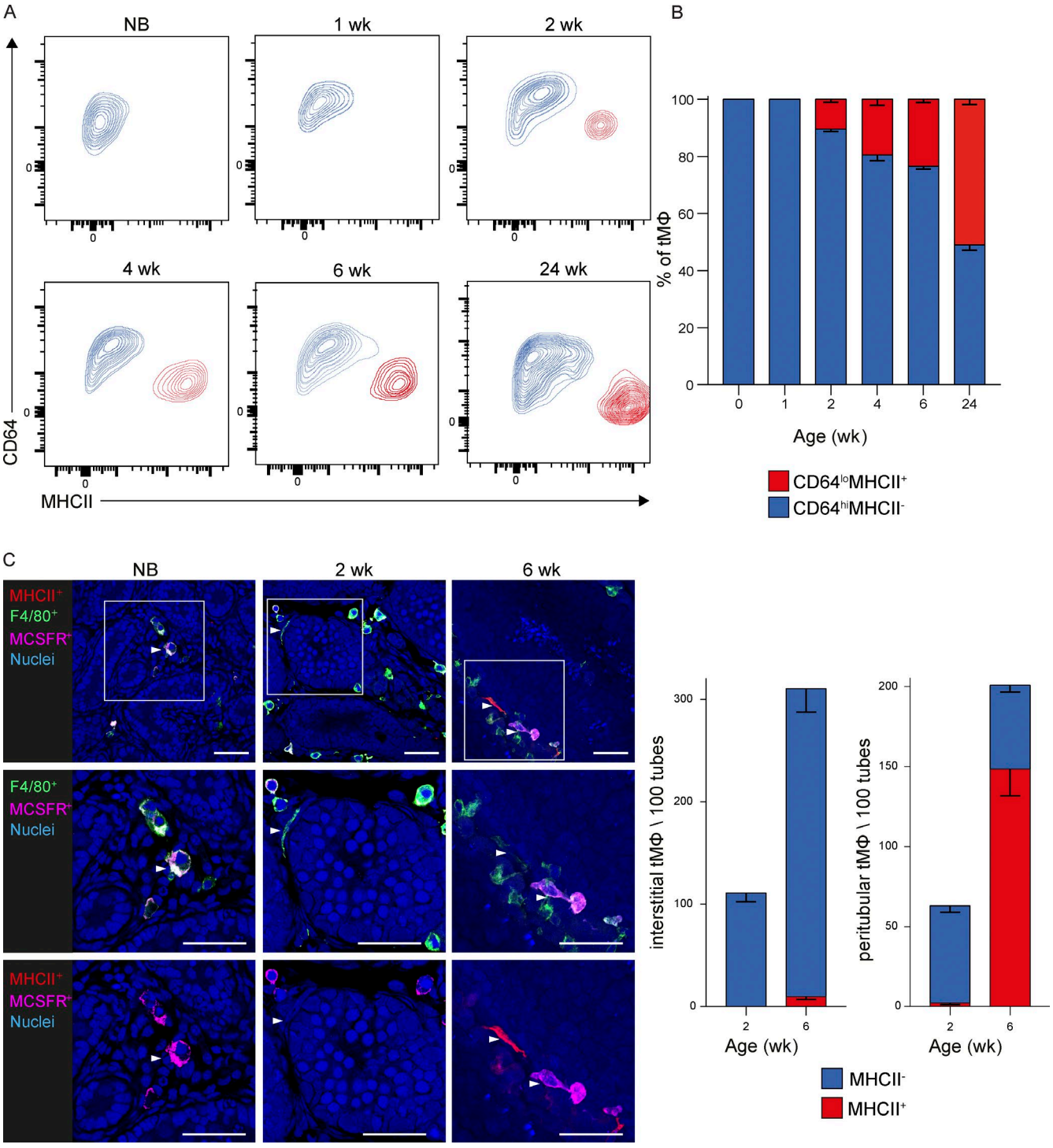

Figure 2. **tMφ populations dynamically change during postnatal development.** (A and B) Analysis of the proportion of CD64^{hi}MHCII^{-} interstitial and CD64^{lo}MHCII^{+} peritubular tMφ from mice of the indicated ages, showing representative FACS plots (A) and mean percentage (B). Error bars represent SEM. *n* = 4–5. All data are representative of at least two independent experiments with four to eight individual mice each. NB, newborn. (C) Analysis of localization and relative numbers of interstitial and peritubular tMφ by IF for M-CSFR and MHCII expression during postnatal development from newborn to 2- and 6-wk-old mice. Nuclear staining by Sytox blue and antigens is shown by the indicated colors. Bars, 40 µm. Representative images (left) and quantification of relative numbers and MHCII expression in interstitial and peritubular populations (right) are shown. Arrowheads show an interstitial macrophage localized in the interstitial space with expression by IF of F4/80 and MCSFR (newborn; left), show peritubular macrophage localization surrounding the tube and

vation genes in both populations (Fig. 1 E). As an exception to this, the expression of only a few genes differed, such as the immunosuppressive M2-type genes *IL-10* and macrophage receptor with collagenous structure (*MARCO*), which were more highly expressed in CD64^{hi}MHCII^{-} interstitial macrophages, and *IL-1b*, which was increased in CD64^{lo} MHCII^{+} peritubular macrophages. Thus, phenotypic characterization by cell-surface markers and mRNA gene expression profiling clearly and consistently identified two distinct interstitial and peritubular tMφ identities.

To investigate the postnatal development of the interstitial and peritubular tMφ populations, we analyzed CD64 and MHCII expression in tMφ from newborn to 24-wk-old mice (Fig. 2, A and B). We observed that all tMφ present at birth were uniformly CD64^{hi}MHCII^{-} (Fig. 2, A and B). This was consistent with IF analysis showing exclusive interstitial localization and expression of M-CSFR but absence of MHCII in tMφ both at birth and at later time points (Fig. 2 C). MHCII^{+} macrophages emerged only after 2 wk of life and further increased thereafter both by FACS and IF analysis (Fig. 2, A–C). IF and confocal imaging analysis allowed a clear distinction of the interstitial macrophage populations with a spherical shape from the peritubular population with an elongated morphology. Interestingly, peritubular macrophages emerged at 2 wk but mostly did not express MHCII yet, whereas a majority was positive at 6 wk, suggesting a potential maturation step after localization to this niche (Fig. 2 C).

Because our data revealed two clearly distinct tMφ populations with different tissue localization, morphology, and surface marker expression emerging at different times during postnatal developmental, we hypothesized that they might also have a distinct developmental origin. To address this question and investigate a potential embryonic origin of the different tMφ populations, we used a genetic fate–mapping model based on CX3CR1-driven tamoxifen (TAM)-inducible Cre recombinase (Cre^{ER}) and R26-yfp reporter mice (Fig. 3 A; Yona et al., 2013; Molawi et al., 2014). TAM-induced pulse labeling at E9 in this model allows identifying cells derived from CX3CR1^{+} yolk sac macrophage progenitors (Hagemeyer et al., 2016) before the onset of definitive hematopoiesis. As a positive control, we used YFP^{+} labeling in microglia, which are exclusively derived from yolk sac macrophage progenitors, remain CX3CR1^{+} throughout development, and self-maintain without contribution of hematopoietic stem cell–derived cells (Ginhoux et al., 2010; Kierdorf et al., 2013). They therefore represent an internal control for maximal CX3CR1 labeling efficiency. E9 pulse labeling with TAM showed a median contribution of 5% from embryonic macrophage progenitors to tMφ in newborn mice, compared with a median of 25% in microglia cells (Fig. 3 B). Using values normalized to microglia to control for interindividual variation in labeling efficiency, we observed that embryonic progenitor contribution to tMφ after birth declined from 20% in neonates to 5% in 6-wk-old mice (Fig. 3 B and S3), similar to what has been reported for other organs (Bain et al., 2014; Molawi et al., 2014; Ensan et al., 2016). IF imaging confirmed that YFP^{+} embryonic progenitor-derived tMφ decreased over time (Fig. 3 C). To determine whether this decline was caused by a decrease in macrophage self-renewal potential over time, as has been observed before in other organs (Bain et al., 2014; Molawi et al., 2014), we determined the proportion of tMφ in S-phase by BrdU incorporation. We observed a strong decline in proliferative capacity of tMφ with age from 8% in neonates to 0% at adulthood (Fig. 3 D). By analyzing BrdU incorporation in YFP^{+} tMφ from E9 pulse-labeled mice, we confirmed that this was also the case specifically for embryonic-derived macrophage progenitor tMφ, which showed a decline from 3% in 2-wk-old mice to 0.5% in 6-wk-old mice of cells in S-phase (Fig. 3 E). Next, we determined to which tMφ subpopulation embryonic macrophage progenitors could contribute. Interestingly, all embryo-derived YFP^{+} tMφ at 6 wk exclusively belonged to the CD64^{hi}MCHII^{-} population and showed no contribution to CD64^{lo}MCHII^{+} tMφ in FACS analysis (Fig. 3 F). IF confirmed that YFP^{+} cells contributed only to the interstitial M-CSFR^{+}MCHII^{-} population but not to M-CSFR^{lo}MCHII^{+} peritubular tMφ (Fig. 3 G). These data demonstrated that embryo-derived macrophages persisted in mouse testis after birth but were restricted to the interstitial CD64^{hi}M-CSFR^{+}MCHII^{-} tMφ population and declined with age.

The lack of embryonic progenitor-derived macrophages in the CD64^{lo}MCHII^{+} peritubular population (Fig. 3) and their emergence only 2 wk after birth (Fig. 2) suggested that this population developed from definitive hematopoiesis in the juvenile animal. Furthermore, the decline of the embryonic progenitor-derived CD64^{hi}M-CSFR^{+}MCHII^{-} interstitial tMφ population could also be caused by a successive replenishment from definitive hematopoiesis-derived cells in the growing animal. To investigate such a potential BM origin of tMφ populations, we established a novel adoptive transfer protocol in neonatal mice (Fig. 4 A). Because the peritubular population appears only 2 wk after birth in the prepuberty period of organ development (Fig. 3 A), classical methods such as BM transplantation into myeloablated mice or parabiosis were not feasible. Therefore, we took a different approach and exploited the fact that the neonatal liver still significantly contributes to hematopoiesis around birth before hematopoietic stem cells transition from this organ to the BM (Orkin and Zon, 2008). We transplanted BM cells directly into the neonatal liver (Hoeffel et al., 2012) without

expressing F4/80 but not MCSFR (2 wk; middle), and display one peritubular macrophage expressing F4/80 and MHCII and an interstitial macrophage with expression of F4/80 and MCSFR (6 wk; right). Data are based on counting 100–1,000 F4/80^{+} cells normalized to 100 seminiferous tubules and represented as mean percentage ± SEM.

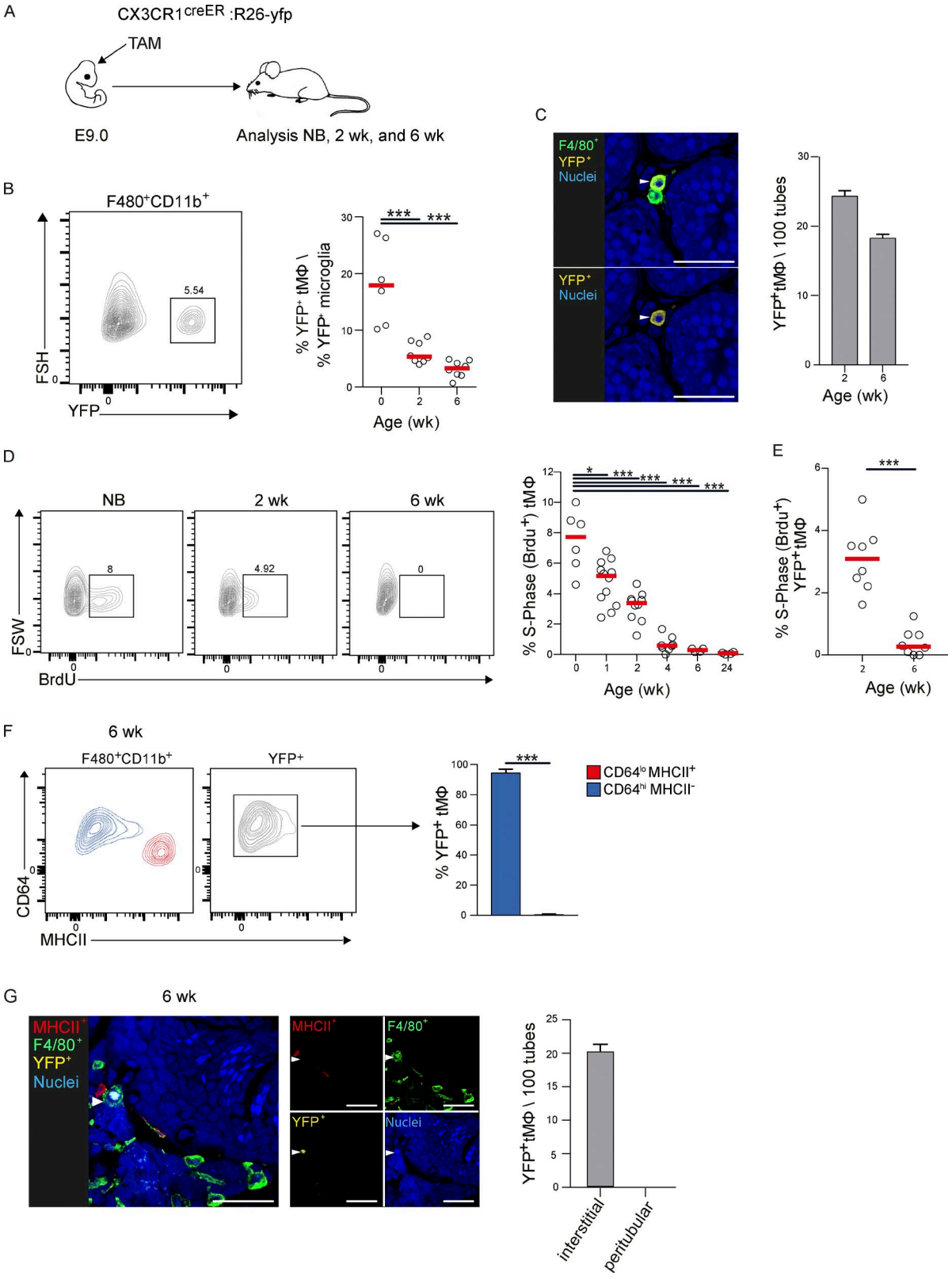

Figure 3. **Embryonic macrophage contribution to tMφ populations in the postnatal testis.** (A) Experimental design. CX3CR1^{CreER}:R26-yfp embryos were treated with TAM at E9 and analyzed on the day of delivery (newborn [NB]) or 2 or 6 wk after birth. (B) Relative abundance of lineage-traced YFP$^+$ cells in F4/80$^+$CD11b$^+$Ly6C$^-$CD11c$^-$ tMφ shown in a representative FACS plot from newborn mice (left) and quantification of relative contribution of YFP$^+$

conditioning, which represents largely physiological conditions during a period of normal organ growth. We transferred BM from mice expressing dTomato from the ubiquitin locus (Ghigo et al., 2013) intrahepatically into newborn pups and analyzed the contribution of BM to tMφ populations 2, 6, and 20 wk after transplantation (Fig. 4 A). 1 wk after transplantation, dTomato$^+$ cells contributed to the hematopoietic stem and progenitor cell (HS/PC) compartment in the BM, confirming the potential of the adoptive transfer protocol to contribute to BM hematopoiesis (Fig. 4 B). We found that transplanted dTomato$^+$ BM already contributed to 14% of CD64^{lo}MHCII$^+$ peritubular macrophages in 2-wk-old mice and to 30% in 6-wk-old mice and further increased in 20-wk-old mice (Fig. 4 C). In contrast, contribution of transplanted dTomato$^+$ BM to the CD64^{hi}MHCII$^-$ interstitial population was negligible at 2 wk, only at 3% by 6 wk, and at 5% at 20 wk (Fig. 4 C). Confocal imaging analysis confirmed that transplanted BM-derived macrophages localized only to the peritubular location at 2 wk further increased at this location by 6 wk and were nearly exclusively MHC II$^+$. No contribution to interstitial macrophages was observed at 2 wk, and only minimal numbers were observed at 6 wk (Fig. 4 D). Together, these observations confirmed that CD64^{lo}MHCII$^+$ peritubular tMφ were exclusively BM derived and that the decline of early embryo-derived macrophages in the CD64^{hi}MHCII$^-$ interstitial population was partially compensated by replenishment from BM-derived cells.

Next, we determined the turnover rate of the two tMφ populations once they were stably established in the adult testis. As both CD64^{hi}MHCII$^-$ interstitial and CD64^{lo}MHCII$^+$ peritubular populations are CX3CR1 positive, we could use CX3CR1^{CreER}:R26-yfp mice to pulse label both populations in adult mice at 8 wk of age by TAM injection (Goldmann et al., 2013) and follow YFP$^+$ cell contribution to both tMφ populations over time (Fig. 5, A and B). FACS showed a nearly constant contribution of YFP$^+$ cells to both CD64^{hi}MCHII$^-$ interstitial and CD64^{lo}MCHII$^+$ peritubular tMφ up to 24 wk after labeling, similar to the stable contribution to microglia cells that served as a positive control (Figs. 5 C and S2).

Here, we have characterized the origin, postnatal development, and turnover of two testis-resident macrophage populations. We identified clearly distinct developmental pathways for the peritubular and interstitial tMφ populations that have been associated with distinct support roles for the function of SSCs (DeFalco et al., 2015) and testosterone-producing Leydig cells (Hutson, 1998; Smith et al., 2015). Macrophages have also been suggested to contribute to the immunosuppressive environment in the testis (Fijak and Meinhardt, 2006; Shechter et al., 2013). Here, we demonstrate that both tMφ populations lack the expression of proinflammatory M1-type genes and express a subset of M2-type polarization genes. Despite the overall similarity, interstitial tMφ might make a stronger contribution because of significantly higher IL-10 expression. We have shown that early embryonic progenitors contribute selectively to the interstitial but not to the peritubular population. Similar to other resident macrophages (Bain et al., 2014; Molawi et al., 2014), the interstitial population shows a decline in self-renewal and a reduction in the contribution of early embryo-derived cells with age. This loss is partially compensated by replenishment from BM-derived macrophages. As this contribution remains relatively small in the adult, the replacement of early embryo-derived cells might already occur early after birth from fetal sources of hematopoiesis. In contrast, the peritubular population only becomes established at 2 wk of age in the prepuberty period and is derived exclusively from BM progenitors. Once established, both populations exhibit a slow turnover and extraordinary long life span in the steady state.

Our observations on peritubular tMφ provide a unique example of a functionally and phenotypically distinct resident macrophage population that develops exclusively from BM-derived progenitors to populate a dedicated niche that only becomes available after birth. Most macrophage populations are of mixed origin because of successive waves of seeding of the developing organ during embryogenesis and after birth from different yolk sac, fetal liver, and BM sources of hematopoiesis (Sieweke and Allen, 2013; Ginhoux and Guilliams, 2016; Perdiguero and Geissmann, 2016). The interstitial tMφ described here fall into this category with mixed embryonic and BM origin. At one extreme end of this spectrum, microglia cells of the brain are exclusively derived from early yolk sac–derived progenitors and do not receive addi-

cells normalized to microglia labeling efficiency at the indicated time points (right). Bars show the median. n = 6–8. (C) Analysis of the contribution of fate-mapped YFP$^+$ cells to F4/80$^+$ tMφ by IF, showing a representative example from a 2-wk-old mouse (left) and quantification of contribution in 2- and 6-wk-old mice (right). Data are based on counting 100–200 YFP$^+$F4/80$^+$ cells normalized to 100 seminiferous tubules. Arrowheads show one YFP$^+$F480$^+$ testicular macrophage (top) and the same cell with only YFP labeling, proving that we can visualized our fate-mapping cells (bottom). Bars, 40 µm. (D) Analysis of proliferation rate of tMφ at the indicated age by BrdU incorporation and flow cytometry 4 h after BrdU injection (i.p), showing representative FACS plots (left) and quantification (right). Bars show the median. n = 4–12. NB, newborn. (E) Analysis of the proliferation rate of fate-mapped YFP tMφ (F4/80$^+$CD11b$^+$Ly6C$^-$CD11c$^-$) in 2- and 6-wk-old mice by BrdU incorporation and flow cytometry 4 h after BrdU injection (i.p.). Bars show the median. n = 8. (F) Analysis of contribution of fate-mapped YFP$^+$ cells to CD64^{hi}MHCII$^-$ interstitial and CD64^{lo}MHCII$^+$ peritubular macrophages in 6-wk-old mice, showing a representative FACS plot (left) and quantification expressed as the median (right). n = 8. (B and D–F) Data were pooled from two independent experiments. (G) Contribution of fate-mapped YFP$^+$ cells to interstitial and peritubular tMφ populations in 6-wk-old mice determined by IF showing representative examples (left) and quantification of cells normalized to 100 seminiferous tubules. Arrowheads show an interstitial fate-mapped YFP$^+$ macrophage localized in the interstitial space with expression by IF of F4/80 and M-CSFR. Bars, 40 µm. Error bars represent SEM. P-values were obtained by Mann-Whitney U tests. *, $P \leq 0.05$; ***, $P \leq 0.0007$.

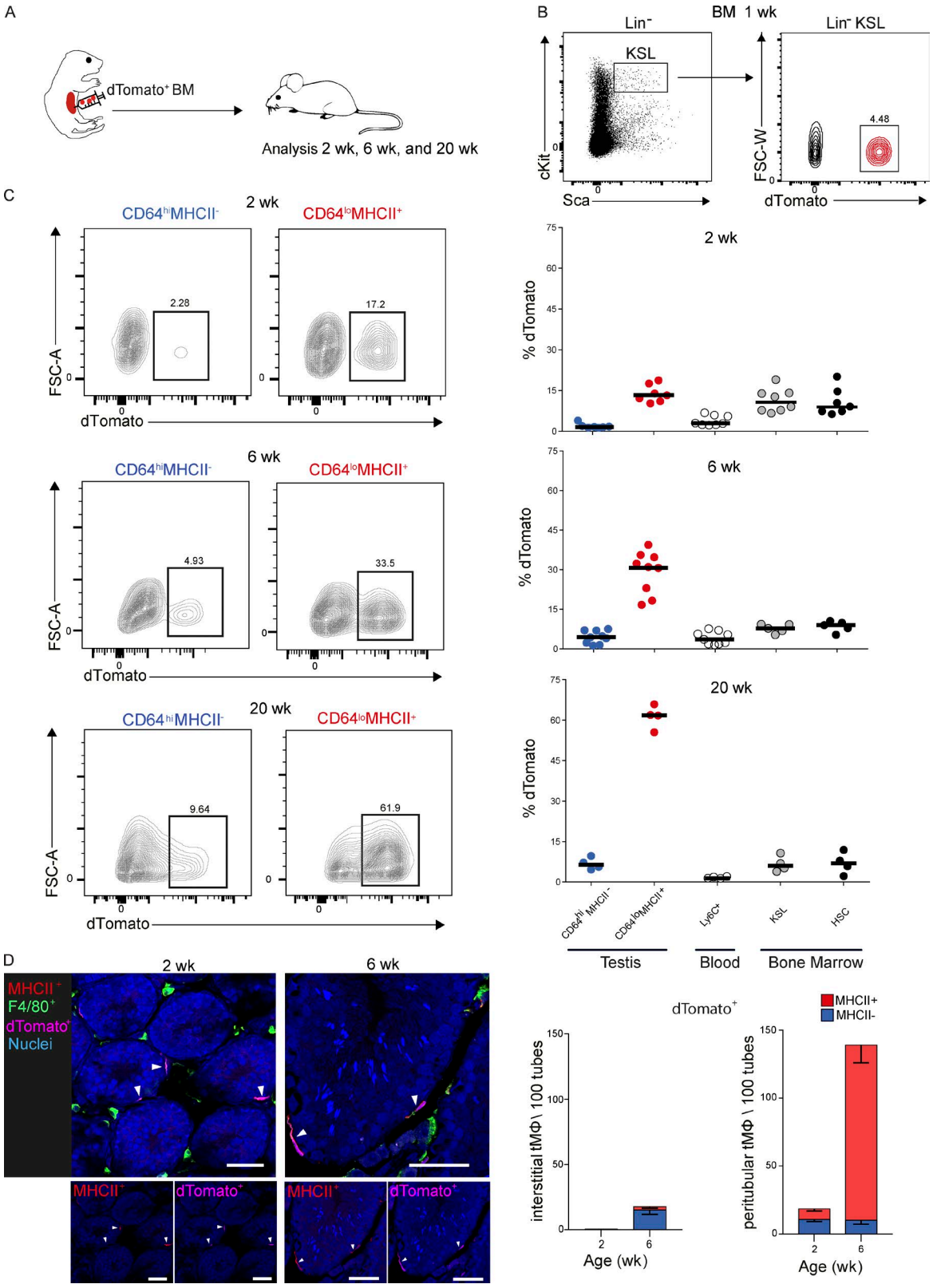

Figure 4. **BM contribution to tMφ populations.** (A) Experimental design. Total dTomato+ BM cells were adoptively transferred by intrahepatic injection into newborn mice and analyzed for contribution to tMφ populations 2, 6, and 20 wk after transplantation. (B) Contribution of dTomato+ BM cells to the HS/PC compartment in BM 1 wk after transplantation. Data are representative of at least two independent experiments. FSC, forward scatter; HSC, hema-

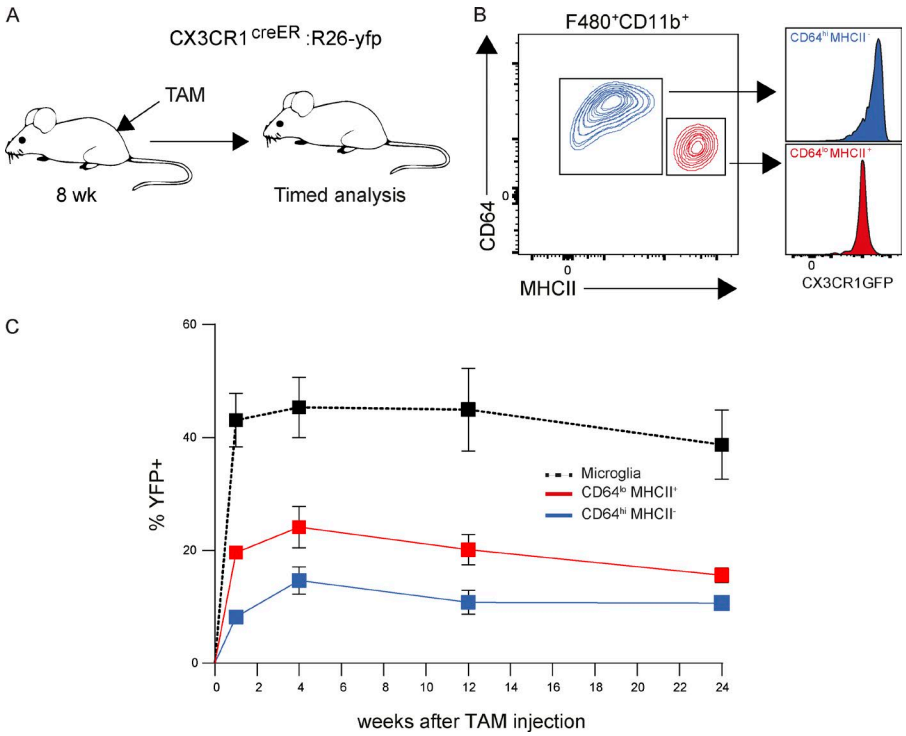

Figure 5. **tMφ populations are long lived.** (A–C) Analysis of tMφ turnover in adult mice using TAM pulse labeling of $CD64^{hi}MHCII^{-}$ interstitial and $CD64^{lo}MHCII^{+}$ peritubular macrophage populations in 8-wk-old $CX3CR1^{CreER}$:R26-yfp mice, showing experimental design (A), CX3CR1 expression in both populations (B), and contribution of labeled YFP^{+} cells to $CD64^{hi}MHCII^{-}$ and $CD64^{lo}MHCII^{+}$ populations at the indicated time points, with microglia contribution shown as a positive control (C). Error bars represent SEM. n = 4–5. Data are representative of two independent experiments.

tional input from other hematopoietic sources in the steady state. Here, we now show that the other extreme also exists for a macrophage niche that only becomes available about 2 wk after birth, when all sources of embryonic hematopoiesis have subsided, and then becomes exclusively populated from BM-derived macrophages. This late seeding is not associated with a short half-life or high turnover that has been described for some short-lived monocyte-derived macrophages that have been labeled as passenger macrophages (Perdiguero and Geissmann, 2016). Therefore, despite their late emergence and BM origin, peritubular tMφ have to be considered a long-lived resident macrophage population.

The testis is unique in that functional maturation and important aspects of organ development only occur after birth in the prepuberty period. M-CSF–deficient mice have reduced numbers of tMφ, defective spermatogenesis, and are infertile (Cohen et al., 1996). Diphtheria toxin–mediated depletion experiments also suggest that macrophages might promote spermatogenesis, possible by directly acting on SSCs found in close proximity to peritubular macrophages (DeFalco et al., 2015). Peritubular macrophages might also play a unique tolerizing role against meiotic germ cell autoantigens that are shed during spermiation. Because a subset of them can pass the Sertoli cell barrier into the interstitial space (Tung et al., 2017), the close proximity of peritubular tMφ and their high expression levels of MHCII might predispose them to present autoantigen to regulatory T cells. We now observed that macrophages only start to populate this specific peritubular location when spermatogenesis is initiated at 2–3 wk of age, although the physical structures of seminiferous tubules are already present long before. This suggests that macrophages might not only affect spermatogonial differentiation and tolerance against autoantigens, but also that, reversely, initiation of spermatogenesis might induce a specific environment enabling the recruitment of a dedicated macrophage population. Together, this highlights the power of the microenvironment in controlling macrophage identity and numbers (Sieweke, 2015; Guilliams and Scott, 2017). It also suggests an intimate link between specific support macrophage and parenchymal cell populations of the organ that reciprocally influence each other's identity and function.

topoietic stem cell; KSL, $Kit^{+}Sca\text{-}1^{+}Lineage^{-}$. (C) Contribution of neonatally transplanted $dTomato^{+}$ BM cells to $CD64^{hi}MHCII^{-}$ interstitial and $CD64^{lo}MHCII^{+}$ peritubular macrophage populations, assessed by flow cytometry at 2, 6, and 20 wk of age, showing FACS plot examples (left) and quantification (right). $Ly6C^{+}$ blood monocyte and BM hematopoietic stem cell contributions are shown as references. Data were pooled from two independent experiments for 2- and 6-wk-old mice (n = 7–9) and are representative of two independent experiments for 20-wk-old mice (n = 4). (D) IF imaging analysis of transplanted $dTomato^{+}$ BM contribution to interstitial and peritubular tMφ in 2- and 6-wk-old mice showing representative images (left) and quantification of MHCII expression (right). Arrowheads show peritubular macrophages after BM transplantation, labeled in tomato and showing or not expressing MHCII. Data are based on counting 100–300 $dTomato^{+}$ $F4/80^{+}$ cells normalized to 100 seminiferous tubules. Errors bars represent SEM. Bars, 40 µm.

MATERIALS AND METHODS

Mice

Wild-type C57BL/6J mice were purchased from Janvier laboratories. All transgenic mice used in this study have a C57BL/6 background. CX3CR1$^{GFP/+}$ mice (Jung et al., 2000), Rosa26-yfp and CX3CR1^{creER} mice (JAX stock no. 20940 B6J.129-Cx3cr1<tm1.1[cre/ERT2]Jung>/J; Yona et al., 2013), and Ubow mice, provided by M. Bajenoff (Centre d'Immunologie de Marseille-Luminy, Marseille, France; Ghigo et al., 2013) were used. Experiments were performed on mice at the indicated age. In vivo procedures were performed under specific pathogen–free conditions following protocols approved by the Ethics Committee of Marseille in accordance with institutional, national, and European regulations (approval nos. APAFIS 3292-2015 1221 09359224 and APAFIS 10545-2017 0710 08253541).

Genetic fate mapping

To genetically fate map progeny of cells expressing CX3CR1, CX3CR1^{CreER} mice were crossed onto R26-yfp mice, and pregnant CX3CR1^{CreER}:R26-yfp females were administered a single dose of TAM (Sigma) at E9. TAM was complemented with progesterone (Sigma), dissolved in ethanol and diluted 10-fold in corn oil (Sigma). The freshly prepared solution was injected intraperitoneally at a dose of 0.1 mg TAM and 0.05 mg progesterone per gram body weight. For induction of Cre recombinase in 8-wk-old CX3CR1^{CreER} R26-yfp mice, 4 mg TAM, dissolved in 200 µl of corn oil, was injected twice subcutaneously 48 h apart.

Neonatal hematopoietic cell transplantation

Total BM was obtained from long bones according to standard procedures. Adult (8–12 wk) Ubow mice that express dTomato under the control of the human ubiquitin–C promoter (Ghigo et al., 2013) were used as donors for BM cells. RBCs from total dTomato BM were lysed using RBC lysis buffer (CliniSciences). Five million cells were injected in 20 µl PBS intrahepatically into newborn pups using a micro-fine syringe with 8-mm needles (Micro-Fine 0.3 ml; BD).

In vivo BrdU incorporation

To assess DNA synthesis as readout for proliferation, mice were pulsed with BrdU (Sigma) for 4 h before euthanization and organ harvest. Mice were administered 0.1 mg BrdU per gram body weight either subcutaneously (newborn pubs) or intraperitoneally. BrdU incorporation was measured using a BrdU Flow kit (BD) according to the manufacturer's instructions.

Leukocyte isolation from mouse tissues

The tunica albuginea of resected testes was opened, and cells were transferred into RPMI medium containing 1 mg/ml Collagenase II (Worthington Biochemicals) and 0.15 mg/ml DNase I (Sigma). Testis-resident leukocytes were obtained through enzymatic digestion at 37°C for 40 min and passage through 70-µm cell strainers (BD Falcon). Brain tissue was macerated and taken up in HBSS containing 0.5% D-glucose (Sigma) and 15 mM Hepes (Life Technologies). The resulting cell suspension was passed through 70-µm cell strainers and subjected to a 70/37/30% Percoll gradient, from which microglia were isolated. Peripheral blood leukocytes were isolated by density centrifugation using Lymphoprep reagent (Stem Cell Technologies) following the manufacturer's instructions.

Flow cytometry

Single-cell suspensions were preincubated with an antibody blocking Fc receptors (TruStain Fx anti-CD16/32; clone 2.4G2; Biolegend). Subsequently, fixable live/dead staining reagents were used according to the manufacturer's instructions (Zombie Dyes; Biolegend). Staining for expression of surface antigens was performed for 20 min at 4°C. The following antibodies were used throughout this study: anti-CD45–BV421 (clone 30F11; Biolegend), anti-F4/80–BV785 (clone BM8; Biolegend), anti-CD11b–BV605 (clone M1/70; BD), anti-CD64–PerCP/Cy5.5 (X54-5/7.1; Biolegend), anti-CD14–APC (Sa2-8; eBioscience), anti-MerTK–biotin (RD Systems), anti-CD11c–BV711 (clone N418; Biolegend), anti-CD115–BV421 (clone AFS98; Biolegend), anti-Ly6C–APC/Cy7 (clone HK1.4; Biolegend), and anti–I-A/I-E (MHCII)–PE/Cy7 (clone M5/114.15.2; Biolegend). Biotinylated antibodies were detected with streptavidin-PE and -BV786 (BD). For HS/PC isolation, total BM cells were depleted from mature cells by staining with biotinylated rat anti–mouse lineage antibody cocktail, followed by streptavidin immunomagnetic microbeads (Miltenyi Biotec). Lineage-negative cells were stained with HS/PC markers: anti-CD117–APC-H7 (clone 2B8; BD), anti-Sca1–PE-Cy5 (clone D7; Biolegend), streptavidin-APC (eBioscience), and LIVE/DEAD Fixable Violet Dead cell dye (Invitrogen) as a viability marker. Data were acquired on an LSRII instrument (BD) and analyzed using FlowJo software (Tree Star). Flow cytometry cell sorting was performed on ARIA and ARIA SORP systems (BD).

IF and confocal imaging

Resected testes were fixed in Antigen-Fix reagent (Diapath) for 2 h at 4°C, washed in phosphate buffer, and dehydrated in a 30% sucrose solution overnight at 4°C. Samples were embedded in TissueTek medium (Sakura Finetek), frozen at −80°C, and cut into 20-µm sections for the entire organ using a cryostat (CM3050S; Leica). Slides were blocked 20 min at room temperature in PBS/2% BSA/1% donkey serum/1% FCS/0.1% saponin and stained overnight at 4°C with the indicated antibodies. The following antibodies were used throughout this study: anti-F4/80–Alexa Fluor 647 (clone BM8; Biolegend), anti-MHCII–efluor450 (clone M5/114.15.2; ebioscience), and anti–M-CSFR (C-20; Santa Cruz). After three washes in PBS/0.05% saponin, anti–M-CSFR antibody was detected with anti–rabbit–Alexa Fluor 594 (Jackson Immunoresearch), and visualization of YFP^{+}

cells was enhanced using an anti-GFP antibody (Life Technologies). Slides were mounted in medium containing Sytox blue dye (Prolong Sytox; Life Technologies). Confocal microscopy acquisitions were performed on a confocal microscope (LSM780; Zeiss) at room temperature, and slides were imaged with a 40×/1.4 oil differential interference contrast objective (Plan-Apochromat). Different lasers were used (405, 488, 561, and 633 nm) to excite the fluorophores (Sytox blue, eFluor 450, Alexa Fluor 488, Alexa Fluor 594, and Alexa Fluor 647). Fluorescence was recorded in individual channels acquired in a sequential mode to avoid cross talk using a highly sensitive 32-channel gallium arsenide phosphide detector. The pinhole was set to 1 airy unit. Image processing was done with ImageJ (National Institutes of Health). Only a median filter was performed on the images to remove salt and pepper noise. For quantification in wild-type mice, macrophages corresponding to a total of 450–680 tubes were counted per individual mouse and scored for localization and expression of M-CSFR and MHCII. Quantification of fate mapped or BM transplantation–derived macrophages was based on scoring 100–200 YFP^+ or 100–500 $Tomato^+$ cells, respectively.

Gene expression analysis by microfluidic real-time PCR

Total mRNA was extracted from FACS-sorted bulk populations of 5,000 cells. RNA extraction and cDNA synthesis were performed with a μMACS one step T7 template kit (Miltenyi). Specific target gene expression was detected according to Fluidigm protocols as previously described (Soucie et al., 2016). In brief, after 10 cycles of cDNA preamplification, microfluidic real-time PCR was performed using Dynamic Array integrated fluidic circuits (Biomark; Fluidigm) with TaqMan gene expression assays (ABI) or primer assay in 96.96 Dynamic Arrays on a BioMark System (Fluidigm). Ct values were calculated from the system's software (BioMark Real-time PCR Analysis; Fluidigm).

Primers used for microfluidic real-time PCR were: *IL10Ra* forward, 5′-CACCACTGAGACTCGCTTCA-3′ and reverse, 5′-CGTCCATTGCTTTCAGAGTCAC-3′; *Soc3* forward, 5′-CCTTCAGCTCCAAAAGCGAG-3′ and reverse, 5′-GCTCTCCTGCAGCTTGCG-3′; *Ccl12* forward, 5′-TCCGGAAGCTGAAGAGCTAC-3′ and reverse, 5′-GTCAGCACAGATCTCCTTATCCA-3′; *Ccl2* forward, 5′-AGCAGCAGGTGTCCCAAA-3′ and reverse, 5′-TTCTTGGGGTCAGCACAGAC-3′; *Ccl6* forward, 5′-ATCGTCGCTATAACCCTCCA-3′ and reverse, 5′-CATGGGATCTGTGTGGCATAA-3′; *CD163* forward, 5′-GCCATAACTGCAGGCACAAA-3′ and reverse, 5′-GTTGGTCAGCCTCAGAGACA-3′; *STAB1* forward, 5′-GTACGGTACCACATCTACAACC-3′ and reverse, 5′-TGGTGAGGACACGTCCTTTA-3′; *Ccl7* forward, 5′-TCTGTGCCTGCTGCTCATA-3′ and reverse, 5′-CATAGCAGCATGTGGATGCA-3′; *Ccl23* forward, 5′-GCTGCACGTCCTTTATTTCCAA-3′ and reverse, 5′-GCAGCTTGGGGTCAGTACA-3′; *Fizz1* forward, 5′-ACTTCTTGCCAATCCAGCTAAC-3′ and reverse, 5′-CAAGCACACCCAGTAGCAGT-3′; *PPARg* forward, 5′-AAGACAACGGACAAATCACCA-3′ and reverse, 5′-GGGGGTGATATGTTTGAACTTG-3′; *TGFBR* forward, 5′-TCTGCATTGCACTTATGCTGA-3′ and reverse, 5′-AAAGGGCGATCTAGTGATGGA-3′; *IL10* forward, 5′-GGCGCTGTCATCGATTTCTC-3′ and reverse, 5′-ATGGCCTTGTAGACACCTTGG-3′; *MARCO* forward, 5′-CCAGGACTTTCAGGTGCCAA-3′ and reverse, 5′-TGGCCAGAAGACCCTTTTCAT-3′; *Socs2* forward, 5′-GGTTGCCGGAGGAACAGTC-3′ and reverse, 5′-GAGCCTCTTTTAATTTCTCTTTGGC-3′; *CXCL13* forward, 5′-GTGTGAATCCTCGTGCCAAA-3′ and reverse, 5′-AGCTTGGGGAGTTGAAGACA-3′; *Ccl20* forward, 5′-TGGGTGAAAAGGGCTGTGAA-3′ and reverse, 5′-TTGGGCTGTGTCCAATTCCA-3′; *VEGFa* forward, 5′-CCAGCACATAGGAGAGATGAG-3′ and reverse, 5′-CTGGCTTTGTTCTGTCTTTCTT-3′; *IL4* forward, 5′-ACGGAGATGGATGTGCCAAA-3′ and reverse, 5′-GAAGCACCTTGGAAGCCCTA-3′; *Arg1* forward, 5′-GGATTGGCAAGGTGATGGAA-3′ and reverse, 5′-CGACATCAAAGCTCAGGTGAA-3′; *Ccl22* forward, 5′-CCTTCTTGCTGTGGCAATTCA-3′ and reverse, 5′-GGCAGCAGATACTGTCTTCCA-3′; *Ccl17* forward, 5′-CAGGAAGTTGGTGAGCTGGTA-3′ and reverse, 5′-CTTGCCCTGGACAGTCAGAA-3′; *Ym1* forward, 5′-TGGCCCACCAGGAAAGTACA-3′ and reverse, 5′-GACCTCAGTGGTCCTTCATTC-3′; *Socs1* forward, 5′-CAACGGAACTGCTTCTTCGC-3′ and reverse, 5′-AGCTCGAAAAGGCAGTCGAA-3′; *IL6* forward, 5′-CGGAAGGGAGACTTACCTTGAA-3′ and reverse, 5′-GCTTTGACTGGCAATCAGGAA-3′; *IL27* forward, 5′-CCCAATGTTTCCCTGACTTTCC-3′ and reverse, 5′-CGAAGTGTGGTAGCGAGGAA-3′; *MMP9* forward, 5′-TCCCCAAAGACCTGAAAACC-3′ and reverse, 5′-GGGTGTAACCATAGCGGTAC-3′; *Nos2* forward, 5′-GCCACCAACAATGGCAACAT-3′ and reverse, 5′-TCGATGCACAACTGGGTGAA-3′; *IL12* forward, 5′-AAACCAGCACATTGAAGACC-3′ and reverse, 5′-GGAAGAAGTCTCTCTAGTAGCC-3′; *Ido1* forward, 5′-ACTTTGTGGACCCAGACACG-3′ and reverse, 5′-GCAGGAGATTCTTTGCCAGC-3′; *IL23a* forward, 5′-ACCAGCGGGACATATGAATCT-3′ and reverse, 5′-AGACCTTGGCGGATCCTTTG-3′; *IL12b* forward, 5′-GGAAGCACGGCAGCAGAATA-3′ and reverse, 5′-AACTTGAGGGAGAAGTAGGAATGG-3′; *CXCL10* forward, 5′-GGGCCATAGGGAAGCTTGAA-3′ and reverse, 5′-GGATTCAGACATCTCTGCTCATCA-3′; *IL1B* forward, 5′-TGGCAACTGTTCCTGAACTCA-3′ and reverse, 5′-GGGTCCGTCAACTTCAAAGAAC-3′; and *GAPDH* forward, 5′-GGCCCTCTGTGTGCTCAAG-3′ and reverse, 5′-CTGATAAAATCTACAGTCATAGGAATGGA-3′.

Online supplemental material

Figs. S1 and S2 describe the gating strategy of tMφ and microglia, respectively. Fig. S3 shows relative contribution of embryonic macrophages to tMφ populations.

ACKNOWLEDGMENTS

We thank Dr. Bajenoff for Ubow mice and the Centre d'Immunologie de Marseille-Luminy (CIML) flow cytometry and mouse house facilities for support. We acknowledge the PICSL imaging facility of the CIML (ImagImm), member of the national infrastructure France-BioImaging supported by the French National Research Agency (ANR-10-INBS-04).

This work was supported by institutional grants from Institut National de la Santé et de la Recherche Médicale, Centre National de la Recherche Scientifique, and Aix-Marseille University to the CIML and grants to M.H. Sieweke from the Agence Nationale de la Recherche (ANR-11-BSV3-0026), Fondation pour la Recherche Médicale (DEQ. 20110421320), and the European Research Council (ERC) under the European Union's Horizon 2020 research and innovation program (grant agreement number 695093 MacAge). M.H. Sieweke is a Berlin Institute of Health–Einstein fellow and Institut National de la Santé et de la Recherche Médicale–Helmholtz group leader.

The authors declare no competing financial interests.

Author contributions: N. Mossadegh-Keller designed and performed experiments, analyzed data, and wrote the manuscript. R. Gentek contributed to data analysis and writing. G. Gimenez performed qPCR gene expression analysis. S. Bigot contributed to FACS experiment design and analysis. S. Mailfert contributed to microscopy experiment design and analysis. M.H. Sieweke conceived and supervised the study, analyzed data, and wrote the manuscript.

Submitted: 8 May 2017
Revised: 16 June 2017
Accepted: 13 July 2017

REFERENCES

Ajami, B., J.L. Bennett, C. Krieger, W. Tetzlaff, and F.M. Rossi. 2007. Local self-renewal can sustain CNS microglia maintenance and function throughout adult life. *Nat. Neurosci.* 10:1538–1543. http://dx.doi.org/10.1038/nn2014

Aziz, A., E. Soucie, S. Sarrazin, and M.H. Sieweke. 2009. MafB/c-Maf deficiency enables self-renewal of differentiated functional macrophages. *Science.* 326:867–871. http://dx.doi.org/10.1126/science.1176056

Bain, C.C., A. Bravo-Blas, C.L. Scott, E.G. Perdiguero, F. Geissmann, S. Henri, B. Malissen, L.C. Osborne, D. Artis, and A.M. Mowat. 2014. Constant replenishment from circulating monocytes maintains the macrophage pool in the intestine of adult mice. *Nat. Immunol.* 15:929–937. http://dx.doi.org/10.1038/ni.2967

Cohen, P.E., O. Chisholm, R.J. Arceci, E.R. Stanley, and J.W. Pollard. 1996. Absence of colony-stimulating factor-1 in osteopetrotic (csfmop/csfmop) mice results in male fertility defects. *Biol. Reprod.* 55:310–317. http://dx.doi.org/10.1095/biolreprod55.2.310

DeFalco, T., I. Bhattacharya, A.V. Williams, D.M. Sams, and B. Capel. 2014. Yolk-sac-derived macrophages regulate fetal testis vascularization and morphogenesis. *Proc. Natl. Acad. Sci. USA.* 111:E2384–E2393. http://dx.doi.org/10.1073/pnas.1400057111

DeFalco, T., S.J. Potter, A.V. Williams, B. Waller, M.J. Kan, and B. Capel. 2015. Macrophages contribute to the spermatogonial niche in the adult testis. *Cell Reports.* 12:1107–1119. http://dx.doi.org/10.1016/j.celrep.2015.07.015

Ensan, S., A. Li, R. Besla, N. Degousee, J. Cosme, M. Roufaiel, E.A. Shikatani, M. El-Maklizi, J.W. Williams, L. Robins, et al. 2016. Self-renewing resident arterial macrophages arise from embryonic $CX3CR1^{+}$ precursors and circulating monocytes immediately after birth. *Nat. Immunol.* 17:159–168. http://dx.doi.org/10.1038/ni.3343

Epelman, S., K.J. Lavine, A.E. Beaudin, D.K. Sojka, J.A. Carrero, B. Calderon, T. Brija, E.L. Gautier, S. Ivanov, A.T. Satpathy, et al. 2014. Embryonic and adult-derived resident cardiac macrophages are maintained through distinct mechanisms at steady state and during inflammation. *Immunity.* 40:91–104. http://dx.doi.org/10.1016/j.immuni.2013.11.019

Fijak, M., and A. Meinhardt. 2006. The testis in immune privilege. *Immunol. Rev.* 213:66–81. http://dx.doi.org/10.1111/j.1600-065X.2006.00438.x

Gautier, E.L., T. Shay, J. Miller, M. Greter, C. Jakubzick, S. Ivanov, J. Helft, A. Chow, K.G. Elpek, S. Gordonov, et al. Immunological Genome Consortium. 2012. Gene-expression profiles and transcriptional regulatory pathways that underlie the identity and diversity of mouse tissue macrophages. *Nat. Immunol.* 13:1118–1128. http://dx.doi.org/10.1038/ni.2419

Ghigo, C., I. Mondor, A. Jorquera, J. Nowak, S. Wienert, S.P. Zahner, B.E. Clausen, H. Luche, B. Malissen, F. Klauschen, and M. Bajénoff. 2013. Multicolor fate mapping of Langerhans cell homeostasis. *J. Exp. Med.* 210:1657–1664. http://dx.doi.org/10.1084/jem.20130403

Ginhoux, F., and M. Guilliams. 2016. Tissue-resident macrophage ontogeny and homeostasis. *Immunity.* 44:439–449. http://dx.doi.org/10.1016/j.immuni.2016.02.024

Ginhoux, F., M. Greter, M. Leboeuf, S. Nandi, P. See, S. Gokhan, M.F. Mehler, S.J. Conway, L.G. Ng, E.R. Stanley, et al. 2010. Fate mapping analysis reveals that adult microglia derive from primitive macrophages. *Science.* 330:841–845. http://dx.doi.org/10.1126/science.1194637

Goldmann, T., P. Wieghofer, P.F. Müller, Y. Wolf, D. Varol, S. Yona, S.M. Brendecke, K. Kierdorf, O. Staszewski, M. Datta, et al. 2013. A new type of microglia gene targeting shows TAK1 to be pivotal in CNS autoimmune inflammation. *Nat. Neurosci.* 16:1618–1626. http://dx.doi.org/10.1038/nn.3531

Gomez Perdiguero, E., K. Klapproth, C. Schulz, K. Busch, E. Azzoni, L. Crozet, H. Garner, C. Trouillet, M.F. de Bruijn, F. Geissmann, and H.R. Rodewald. 2015. Tissue-resident macrophages originate from yolk-sac-derived erythro-myeloid progenitors. *Nature.* 518:547–551. http://dx.doi.org/10.1038/nature13989

Guilliams, M., and C.L. Scott. 2017. Does niche competition determine the origin of tissue-resident macrophages? *Nat. Rev. Immunol.* 17:451–460. http://dx.doi.org/10.1038/nri.2017.42

Hagemeyer, N., K. Kierdorf, K. Frenzel, J. Xue, M. Ringelhan, Z. Abdullah, I. Godin, P. Wieghofer, M.J. Costa Jordão, T. Ulas, et al. 2016. Transcriptome-based profiling of yolk sac-derived macrophages reveals a role for Irf8 in macrophage maturation. *EMBO J.* 35:1730–1744. http://dx.doi.org/10.15252/embj.201693801

Hashimoto, D., A. Chow, C. Noizat, P. Teo, M.B. Beasley, M. Leboeuf, C.D. Becker, P. See, J. Price, D. Lucas, et al. 2013. Tissue-resident macrophages self-maintain locally throughout adult life with minimal contribution from circulating monocytes. *Immunity.* 38:792–804. http://dx.doi.org/10.1016/j.immuni.2013.04.004

Hoeffel, G., Y. Wang, M. Greter, P. See, P. Teo, B. Malleret, M. Leboeuf, D. Low, G. Oller, F. Almeida, et al. 2012. Adult Langerhans cells derive predominantly from embryonic fetal liver monocytes with a minor contribution of yolk sac–derived macrophages. *J. Exp. Med.* 209:1167–1181. http://dx.doi.org/10.1084/jem.20120340

Hutson, J.C. 1998. Interactions between testicular macrophages and Leydig cells. *J. Androl.* 19:394–398.

Jung, S., J. Aliberti, P. Graemmel, M.J. Sunshine, G.W. Kreutzberg, A. Sher, and D.R. Littman. 2000. Analysis of fractalkine receptor CX_3CR1 function by targeted deletion and green fluorescent protein reporter gene insertion. *Mol. Cell. Biol.* 20:4106–4114. http://dx.doi.org/10.1128/MCB.20.11.4106-4114.2000

Kierdorf, K., D. Erny, T. Goldmann, V. Sander, C. Schulz, E.G. Perdiguero, P. Wieghofer, A. Heinrich, P. Riemke, C. Hölscher, et al. 2013. Microglia emerge from erythromyeloid precursors via Pu.1- and Irf8-dependent pathways. *Nat. Neurosci.* 16:273–280. http://dx.doi.org/10.1038/nn.3318

Mass, E., I. Ballesteros, M. Farlik, F. Halbritter, P. Günther, L. Crozet, C.E. Jacome-Galarza, K. Händler, J. Klughammer, Y. Kobayashi, et al. 2016. Specification of tissue-resident macrophages during organogenesis. *Science.* 353:aaf4238. http://dx.doi.org/10.1126/science.aaf4238

Molawi, K., Y. Wolf, P.K. Kandalla, J. Favret, N. Hagemeyer, K. Frenzel, A.R. Pinto, K. Klapproth, S. Henri, B. Malissen, et al. 2014. Progressive

replacement of embryo-derived cardiac macrophages with age. *J. Exp. Med.* 211:2151–2158. http://dx.doi.org/10.1084/jem.20140639

Murray, P.J., J.E. Allen, S.K. Biswas, E.A. Fisher, D.W. Gilroy, S. Goerdt, S. Gordon, J.A. Hamilton, L.B. Ivashkiv, T. Lawrence, et al. 2014. Macrophage activation and polarization: nomenclature and experimental guidelines. *Immunity.* 41:14–20. http://dx.doi.org/10.1016/j.immuni.2014.06.008

Orkin, S.H., and L.I. Zon. 2008. Hematopoiesis: an evolving paradigm for stem cell biology. *Cell.* 132:631–644. http://dx.doi.org/10.1016/j.cell.2008.01.025

Perdiguero, E.G., and F. Geissmann. 2016. The development and maintenance of resident macrophages. *Nat. Immunol.* 17:2–8. http://dx.doi.org/10.1038/ni.3341

Schulz, C., E. Gomez Perdiguero, L. Chorro, H. Szabo-Rogers, N. Cagnard, K. Kierdorf, M. Prinz, B. Wu, S.E. Jacobsen, J.W. Pollard, et al. 2012. A lineage of myeloid cells independent of Myb and hematopoietic stem cells. *Science.* 336:86–90. http://dx.doi.org/10.1126/science.1219179

Shechter, R., A. London, and M. Schwartz. 2013. Orchestrated leukocyte recruitment to immune-privileged sites: absolute barriers versus educational gates. *Nat. Rev. Immunol.* 13:206–218. http://dx.doi.org/10.1038/nri3391

Sieweke, M.H. 2015. Waddington's valleys and Captain Cook's islands. *Cell Stem Cell.* 16:7–8. http://dx.doi.org/10.1016/j.stem.2014.12.009

Sieweke, M.H., and J.E. Allen. 2013. Beyond stem cells: self-renewal of differentiated macrophages. *Science.* 342:1242974. http://dx.doi.org/10.1126/science.1242974

Smith, L.B., P.J. O'Shaughnessy, and D. Rebourcet. 2015. Cell-specific ablation in the testis: what have we learned? *Andrology.* 3:1035–1049. http://dx.doi.org/10.1111/andr.12107

Soucie, E.L., Z. Weng, L. Geirsdóttir, K. Molawi, J. Maurizio, R. Fenouil, N. Mossadegh-Keller, G. Gimenez, L. VanHille, M. Beniazza, et al. 2016. Lineage-specific enhancers activate self-renewal genes in macrophages and embryonic stem cells. *Science.* 351:aad5510. http://dx.doi.org/10.1126/science.aad5510

Tamoutounour, S., S. Henri, H. Lelouard, B. de Bovis, C. de Haar, C.J. van der Woude, A.M. Woltman, Y. Reyal, D. Bonnet, D. Sichien, et al. 2012. CD64 distinguishes macrophages from dendritic cells in the gut and reveals the Th1-inducing role of mesenteric lymph node macrophages during colitis. *Eur. J. Immunol.* 42:3150–3166. http://dx.doi.org/10.1002/eji.201242847

Tung, K.S., J. Harakal, H. Qiao, C. Rival, J.C. Li, A.G. Paul, K. Wheeler, P. Pramoonjago, C.M. Grafer, W. Sun, et al. 2017. Egress of sperm autoantigen from seminiferous tubules maintains systemic tolerance. *J. Clin. Invest.* 127:1046–1060. http://dx.doi.org/10.1172/JCI89927

van Furth, R., and Z.A. Cohn. 1968. The origin and kinetics of mononuclear phagocytes. *J. Exp. Med.* 128:415–435. http://dx.doi.org/10.1084/jem.128.3.415

Winnall, W.R., and M.P. Hedger. 2013. Phenotypic and functional heterogeneity of the testicular macrophage population: a new regulatory model. *J. Reprod. Immunol.* 97:147–158. http://dx.doi.org/10.1016/j.jri.2013.01.001

Wynn, T.A., A. Chawla, and J.W. Pollard. 2013. Macrophage biology in development, homeostasis and disease. *Nature.* 496:445–455. http://dx.doi.org/10.1038/nature12034

Yona, S., K.-W. Kim, Y. Wolf, A. Mildner, D. Varol, M. Breker, D. Strauss-Ayali, S. Viukov, M. Guilliams, A. Misharin, et al. 2013. Fate mapping reveals origins and dynamics of monocytes and tissue macrophages under homeostasis. *Immunity.* 38:79–91. http://dx.doi.org/10.1016/j.immuni.2012.12.001